Title

Incorporation of an Asymmetric Mo-Fe-S Cluster as an Artificial Cofactor into Nitrogenase.

Journal

ChemBioChem, 23(19)

Authors

Tanifuji, Kazuki
Jasniewski, Andrew
Lee, Chi
et al.

Publication Date

2022-10-06

DOI

10.1002/cbic.202200384

Peer reviewed

HHS Public Access

Author manuscript

Chembiochem. Author manuscript; available in PMC 2023 October 06.

Published in final edited form as:

Chembiochem. 2022 October 06; 23(19): e202200384. doi:10.1002/cbic.202200384.

Incorporation of an Asymmetric Mo-Fe-S Cluster as an Artificial Cofactor into Nitrogenase

Kazuki Tanifuji[a],[b], **Andrew J. Jasniewski**[a], **Chi Chung Lee**[a], **Joseph B. Solomon**[a],[c], **Takayuki Nagasawa**[d], **Yasuhiro Ohki**[b], **Kazuyuki Tatsumi**[d], **Britt Hedman**[e], **Keith O. Hodgson**[e],[f], **Yilin Hu**[a], **Markus W. Ribbe**[a],[c]

[a]Department of Molecular Biology & Biochemistry, University of California, Irvine, Irvine, CA 92697-3900 (USA)

[b]Institute for Chemical Research, Kyoto University, Gokasho, Uji, Kyoto 611-0011 (Japan)

[c]Department of Chemistry, University of California, Irvine, Irvine, CA 92697-2025 (USA)

[d]Department of Chemistry, Graduate School of Science and Research Center for Materials Science, Nagoya University, Furo-cho, Chikusa-ku, Nagoya 464-8602 (Japan)

[e]Stanford Synchrotron Radiation Lightsource, SLAC National Accelerator Laboratory, Stanford University, Menlo Park, CA 94025 (USA)

[f]Department of Chemistry, Stanford University, Stanford, CA 94305 (USA)

Abstract

Nitrogenase employs a sophisticated electron transfer system and a Mo-Fe-S-C cofactor, designated the M-cluster [(cit)$MoFe_7S_9C$]), to reduce atmospheric N_2 to bioaccessible NH_3. Previously, we have shown that the cofactor-free form of nitrogenase can be repurposed as a protein scaffold for the incorporation of a synthetic Fe-S cluster $[Fe_6S_9(SEt)_2]^{4-}$. Here, we demonstrate the utility of an asymmetric Mo-Fe-S cluster $[Cp^*MoFe_5S_9(SH)]^{3-}$ as an alternative artificial cofactor upon incorporation into the cofactor-free nitrogenase scaffold. The resultant semi-artificial enzyme catalytically reduces C_2H_2 to C_2H_4, and CN^- into short-chain hydrocarbons, yet it is clearly distinct in activity from its $[Fe_6S_9(SEt)_2]^{4-}$-reconstituted counterpart, pointing to the possibility to employ molecular design and cluster synthesis strategies to further develop semi-artificial or artificial systems with desired catalytic activities.

Graphical Abstract

yilinh@uci.edu, mribbe@uci.edu.

Supporting information for this article is given via a link at the end of the document.

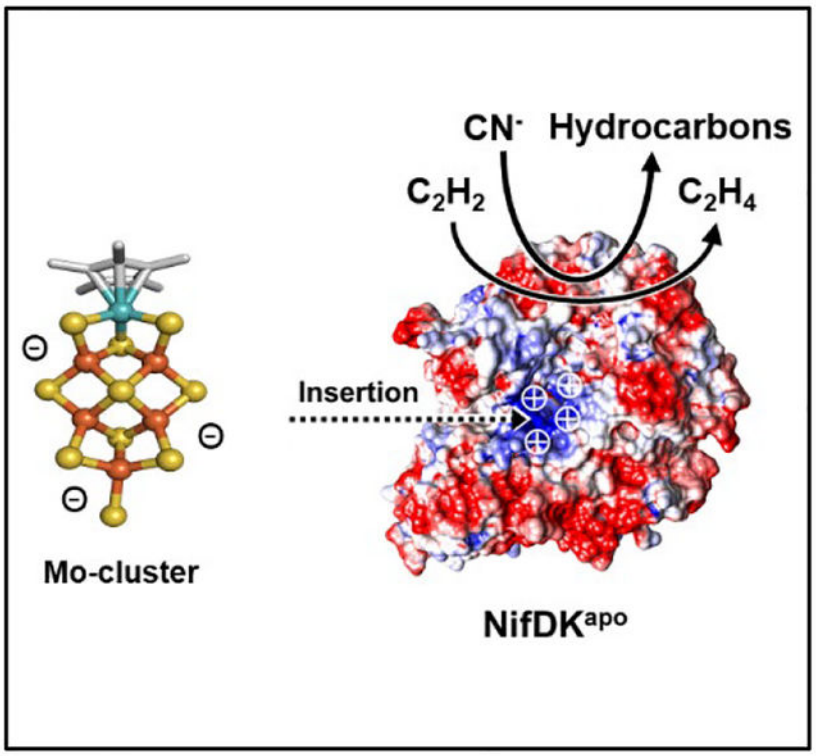

Incorporation of a synthetic asymmetric Mo-Fe-S cluster, [Cp*MoFe5 S9(SH)] $^{3-}$, into the active site of the cofactor-free nitrogenase scaffold results a semi-artificial enzyme that catalytically reduces C_2H_2 to C_2H_4, and CN^- into short-chain hydrocarbons.

Keywords

Nitrogenase; Artificial enzyme; Synthetic Mo-Fe-S cluster; C1 substarate reduction; Hydrocarbons

INTRODUCTION

Multi-electron redox reactions are commonly used in biological processes to cleave strong multiple bonds of small molecules. The typical strategy employed by nature in these reactions involves embedding cofactors at the active sites of the protein scaffolds and delivering reducing equivalents via electron relays to the substrates bound at the buried active-site cofactors.[1] Such a strategy allows enzymes to isolate reactive cofactors from the surrounding environments and thereby capture and convert substrates without interference from unproductive side reactions, such as decomposition of cofactors and competitive formation of byproducts. One exemplary biological system in this genre is nitrogenase, which reduces atmospheric N_2 into bioavailable NH_3 at ambient conditions. The best studied molybdenum nitrogenase comprises two components: a γ_2-homodimeric, reductase component (NifH), which contains a redox-active, subunit-bridging [Fe_4S_4] cluster and an ATP-binding site per subunit; and an $\alpha_2\beta_2$-heterotetrameric, catalytic component (NifDK), which contains a [Fe_8S_7] cluster (P-cluster) at the α/β-subunit interface and a

[(cit)$MoFe_7S_9C$] cluster (M-cluster; cit, *R*-homocitrate).[2–7] The catalytic action of this enzyme initiates from NifH, which interacts with NifDK and transfers an electron from the [Fe_4S_4] cluster to the active-site M-cluster via the P-cluster of NifDK (Figure S1A).[3–5] Every electron transfer event from NifH to NifDK is coupled with ATP hydrolysis, followed by detachment of NifH from NifDK, whereby the reducing equivalents are retained at the active-site M-cluster of NifDK to enable substrate reduction.[2–5]

The inorganic core of the M-cluster consists of [$MoFe_3S_3C$] and [Fe_4S_3C] cubes that are bridged by an interstitial μ_6-C atom and three μ_3-S atoms (Figure 1A, Figure S2A),[6,7] 3 and the terminal Mo and Fe atoms of the cluster is ligated by a His and a Cys residue, respectively, to the NifDK scaffold. Since an M-cluster-free form of NifDK ($NifDK^{apo}$) can be generated via disruption of the cofactor biosynthesis pathway,[8,9] it is conceivable that incorporation of non-native materials into the M-cluster binding site would allow us to repurpose the protein scaffold and the sophisticated electron transfer system of this enzyme. Previously, we have taken a simplistic approach to determine the utility of a synthetic cofactor-substitute based on the structure and size of the M-cluster[10] and successfully combined a synthetic mimic of the M-cluster—designated the Fe6-cluster ($[Fe_6S_9(SEt)_2]^{4-}$) [11]—with the M-cluster-free $NifDK^{apo}$ into a semi-artificial enzyme.[12] Having a [Fe_6S_9] core with an atomic arrangement closely related to the M-cluster, the Fe-cluster can be viewed as an M-cluster variant with an Fe-(μ_2-S)-Fe bridge removed and its μ_6-C substituted with a μ_4-S atom (Figure S2B).[11] Upon reconstitution of $NifDK^{apo}$ with $[Fe_6S_9(SEt)_2]^{4-}$, the resultant protein (designated $NifDK^{Fe6}$) exhibited an increased Fe content concomitant with an acquired catalytic activity in conducting ATP- and NifH-dependent C_2H_2 reduction like its wild-type NifDK counterpart.[12] In addition, $NifDK^{Fe6}$ was capable of catalyzing C_2H_2 and CN^- reduction into short-chain hydrocarbons in an ATP-independent manner in reactions similar to those catalyzed by the wild-type NifDK.[12]

Motivated by our success in combining the Fe6-cluster with the NifDK scaffold, we set out to explore the possibility of incorporating a Mo-containing synthetic cluster as an artificial cofactor into the active site of nitrogenase. Along this line of effort, we have previously reported the synthesis of a so-called Mo-cluster ($[Cp^*MoFe_5S_9(SH)]^{3-}$; Cp*, $C_5(CH_3)_5$), an asymmetric Mo-Fe-S analog of the Fe6-cluster ($[Fe_6S_9(SEt)_2]^{4-}$) that mimics the topology of the native M-cluster (Figure 1B and C, Figure S2C), as well as the ability of the solvent-extracted M-cluster to reduce C_1 substrates (CN^-, CO, CO_2) to short-chain hydrocarbons in a DMF/THF solvent mixture.[13] Given the structural similarity between the Mo- and Fe6-clusters (Figure S2B and C), it is likely that the active site of NifDK, which is capable of housing the Fe6-cluster, is of sufficient size to accommodate the Mo-cluster. Moreover, the Mo-cluster is negatively charged, which could facilitate the incorporation of this cluster into the cluster binding site of NifDK via a positively charged cofactor insertion funnel (Figure 1D). Such an electrostatic interaction between the cofactor and protein scaffold has been proposed to drive the site-specific incorporation of the native M-cluster into NifDK[9] and this scenario may very well be duplicated in the case of the synthetic Mo-cluster.

RESULTS and DISCUSSION

We set out to explore the utility of the asymmetric Mo-cluster as an artificial cofactor in reconstituting the cofactor-free nitrogenase scaffold, which would allow us to generate a semi-synthetic nitrogenase mimic with analogous catalytic activities. To accomplish this goal, excess Mo-clusters were mixed with His-tagged $NifDK^{apo}$ in an aqueous buffer at pH 8.0, yielding a dark brown solution. Subsequent purification of the His-tagged protein from this mixture by affinity chromatography resulted in a dark brown protein species, suggesting a successful reconstitution of $NifDK^{apo}$ with the Mo-cluster. Metal analysis of the purified protein species (designated $NifDK^{Mo}$) by inductively coupled plasma optical emission spectroscopy (ICP-OES) revealed Fe and Mo contents of 31.4±3.4 and 3.9±0.3 atoms per $NifDK^{Mo}$ tetramer, respectively, as compared to the Fe and Mo contents of 15.2±1.4 and 0.2±0.1 atoms per $NifDK^{apo}$ tetramer, respectively. The increase in the Fe and Mo contents of $NifDK^{Mo}$ —by 16.2 and 3.7 atoms per tetramer, respectively—from those of $NifDK^{apo}$ implies incorporation of ~4 Mo-clusters into the protein scaffold, yet there are two cofactor-binding sites that could only house two Mo-clusters per $NifDK^{Mo}$ tetramer. Thus, some of the incorporated Mo-clusters may be attached elsewhere due to a lack of available coordinating residues at the active sites and, therefore, are more accessible to bathophenanthroline disulfonate (BPS), a strong chelator of Fe with a relatively large, rigid molecular structure.[14]

Indeed, treatment of $NifDK^{Mo}$ with BPS resulted in an extraction of 22.6±1.1 Fe atoms per $NifDK^{Mo}$ tetramer; in comparison, the same treatment of $NifDK^{WT}$ resulted in an extraction of only 12.2±1.1 Fe atoms per $NifDK^{WT}$ tetramer. The chelation-accessible Fe atoms of $NifDK^{WT}$ have previously been assigned to the unprotected Fe atoms of the P-cluster that are relatively exposed at the α/β-subunit interface of NifDK.[13] Subtraction of the Fe atoms associated with the P-cluster (12.2) from the total Fe atoms of $NifDK^{Mo}$ (22.6) yielded 10.4 Fe atoms associated with the chelation-accessible Mo-cluster in $NifDK^{Mo}$. Given the Fe content of the Mo-cluster (5 Fe atoms per cluster), this observation suggests that two Mo-clusters are present at the protein surface and more exposed to the solvent; whereas the other two Mo-clusters are protected from the solvent upon incorporation into the cofactor binding sites. Interestingly, re-purification of $NifDK^{Mo}$ after incubation with additional Mo-clusters resulted in no change in the cluster content of the protein (~4 Mo-clusters), implying that the solvent-exposed Mo-clusters are likely associated with defined binding sites and not randomly attached at the protein surface, as the latter scenario would have resulted in an increase in the Mo content of $NifDK^{Mo}$ following incubation with extra Mo-clusters.

Subsequent Fe and Mo K-edge x-ray absorption spectroscopy analyses of $NifDK^{Mo}$ provided additional evidence for the incorporation of the Mo-cluster into the NifDK protein scaffold. The Fe K-edge EXAFS data of $NifDK^{Mo}$ is best fit with 4 Fe–S scatterers at 2.28 Å, either without inclusion of any Fe---Fe scattering pair or with inclusion of one Fe---Fe scatterer at 2.71 Å, although the latter fit shows a relatively high σ^2 value that likely originates from an increased Fe-Fe distance distribution introduced by the presence of a large amount of Fe atoms in the Mo- and P-clusters of $NifDK^{Mo}$ (Figure 2A and B, Table S1). It is interesting to note the slight deviation of the average Fe---Fe distance of $NifDK^{Mo}$ (2.71 Å) from the crystallographically derived, average Fe---Fe distance in the isolated

Mo-cluster (2.74 Å), which could be attributed to an impact of protein environment on the Mo-cluster upon insertion. Consistent with this observation, the Fe K-edge EXAFS data of the cofactor-deficient $NifDK^{apo}$ is best fit with 3 Fe–S scatterers at 2.31 Å, with inclusion of Fe---Fe scattering pairs at 2.53 Å and 2.76 Å (Figure 2A and B, Table S2), an assignment that is clearly different from that of the 'cofactor'-replete $NifDK^{Mo}$. Such distinctions between the Fe K-edge data of $NifDK^{Mo}$ and $NifDK^{apo}$, and between those of $NifDK^{Mo}$ and the isolated Mo-cluster, are consistent with the incorporation of the Mo-cluster into a sulfur-rich environment within the NifDK protein scaffold.

The incorporation of Mo-cluster into NifDK is further supported by the observation that the Mo K-edge data of $NifDK^{Mo}$ is qualitatively reminiscent of those of $NifDK^{WT}$, both of which are highlighted by strong FT features at R+Δ~1.8 Å and 2.3 Å, with a weaker feature at R+Δ~3 Å (Figure 2C and D, Table S3). Similar to that observed in $NifDK^{WT}$, the R+Δ~1.8 Å feature of $NifDK^{Mo}$ is best fit with Mo–S scatterers at 2.28 Å, although it also requires inclusion of Mo–C (with C originating from its Cp* ligand) at 2.24 Å. The Mo center in $NifDK^{Mo}$ maintains certain structural metrics of that in the isolated Mo-cluster, with the FT feature at R+Δ~2.3 Å fit with two Mo---Fe scatterers at 2.72 Å, and the weaker FT feature fit with Mo---C scatterers at 3.45 Å, both of which are consistent with the distances derived from the crystallographic studies of the isolated Mo-cluster. However, the number of Mo–S scatterers in $NifDK^{Mo}$ is lower than the number of sulfide ligands bound to the isolated Mo-cluster, and the Mo–C distance in $NifDK^{Mo}$ is much shorter than the crystallographically determined, average Mo–C (with C originating from its Cp* ligand) distance of 2.39 Å in the isolated Mo-cluster. The similarity between the Mo K-edge data of $NifDK^{Mo}$ and $NifDK^{WT}$, combined with the distinction between those of $NifDK^{Mo}$ and the isolated Mo-cluster, again points to the successful incorporation of the Mo-cluster into the NifDK protein scaffold.

Excitingly, $NifDK^{Mo}$ was capable of reducing C_2H_2 into C_2H_4 in presence of NifH, ATP and dithionite in a reaction similar to that catalyzed by its $NifDK^{WT}$ counterpart, generating 344±6 nmol C_2H_4/mg protein over 30 min that corresponded to a turnover number (TON) of 76 (Figure 3A). Importantly, the formation of C_2H_4 was not observed in the absence of NifH and/or ATP, suggesting that the electrons required for the reaction were delivered from the $[Fe_4S_4]$ cluster of NifH to the incorporated Mo-cluster. Moreover, as catalysis by nitrogenase requires coordination between a number of suitably placed elements for electron delivery in the direction of $[Fe_4S_4]$ cluster→P-cluster→M-cluster, the fact that $NifDK^{Mo}$ mimics $NifDK^{WT}$ in catalyzing the NifH/ATP-dependent substrate reduction implies a proper incorporation of the Mo-clusters at the cofactor binding sites that allows electron delivery in the direction of $[Fe_4S_4]$ cluster→P-cluster→Mo-cluster. It should be noted, however, that while NifDK provides $Cys^{\alpha.275}$ and $His^{\alpha.442}$ as the two coordinating ligands for the native M-cluster, it is likely that only $Cys^{\alpha.275}$ interacts with the incorporated, synthetic Mo-cluster due to a lack of readily exchangeable ligands in the Mo-cluster except for the terminal -SH group.

Under ATP-free conditions, the activity of C_2H_2 reduction by $NifDK^{Mo}$ improved drastically when Eu^{II}-DTPA (DTPA, diethylenetriamine pentaacetate) was used as a reductant to drive the reaction (Figure 3B).[15] Eu^{II}-DTPA has a highly negative redox potential ($E^{O'}_{1/2}$ =

−1.14 V *vs.* SHE at pH 8.0) and is known to mediate electron transfer towards NifDK in the absence of NifH and ATP (Figure S1B).[12] Upon incubation with 20 mM Eu^{II}-DTPA, $NifDK^{Mo}$ converted C_2H_2 into C_2H_4 at a yield of 3198 ±486 nmol C_2H_4/mg protein over 30 min, which corresponded to a TON of 704 per NifDK tetramer. The formation of C_2H_4 increased linearly for ~15 min and reached a plateau at ~30 min. It is notable that, under both ATP-dependent and ATP-independent conditions, the formation of C_2H_4 by $NifDK^{Mo}$ showed similar patterns of time dependency even though the specific yields under these conditions differed by an order of magnitude. This observation may reflect a rate-determining factor of electron transfer in the catalytic cycle of the artificial NifH/$NifDK^{Mo}$ enzyme system. Specifically, a somewhat inefficient docking between NifH and $NifDK^{Mo}$, owing to the incorporation of an unnatural cofactor into the latter protein, could contribute to an inefficient electron transfer and, consequently, a lower yield of products in the ATP-dependent reaction. In addition, the redox potential of the synthetic Mo-cluster relative to those of its 'upstream' partners—the [Fe_4S_4] cluster (of NifH) and the P-cluster (of NifDK)—could also affect the efficiency of electron transfer in this artificial system.

Other than C_2H_2, $NifDK^{Mo}$ was also capable of catalyzing ATP-independent reduction of CN^- in the presence of Eu^{II}-DTPA. Incubation of $NifDK^{Mo}$ with 10 mM CN^- and 20 mM Eu^{II}-DTPA resulted in the formation of C_1-C_3 hydrocarbons (Figure 4A). Labeling of CN^- with ^{13}C gave rise to the expected mass shifts of C_1, C_2, and C_3 products by 1, 2, and 3, respectively, in GC-MS analysis (Figure 4B), confirming CN^- as the C source of the hydrocarbon products. The yields of products generated within 60 min were 79 (CH_4), 11.5 (C_2H_4), 6.1 (C_2H_6), 2.4 (C_3H_6), and 1.1 (C_3H_8) nmol/mg protein, respectively, which amounted to a total of 125 nmol reduced C/mg protein or a TON of 27. The mole fractions of the reduced C in products were 0.63 for the C_1 product (CH_4), 0.28 for the C_2 products (C_2H_4 and C_2H_6), and 0.09 for the C_3 products (C_3H_6 and C_3H_8). The preferred CH_4 production in this reaction is consistent with a higher yield of C_2 products than C_3 products, both of which point to a faster reaction rate of product release than continued C–C coupling. In addition, production of alkenes in this reaction is favored over production of the corresponding alkanes, which is similar to the preferred olefin production in the iron catalyst-based Fischer-Tropsch synthesis of hydrocarbon products.[16] Assuming that the hydrocarbon formation by $NifDK^{Mo}$ proceeds through metal-alkyl species, the higher alkene yields could reflect a more favorable β-hydride elimination in product release than a protonation or reductive elimination of the alkyl groups.

The ability of $NifDK^{Mo}$ to catalyze substrate reduction, either under ATP-dependent or ATP-independent conditions, could be attributed to the physiochemical properties of the synthetic Mo-cluster itself as well as its interaction with the protein scaffold. Upon incorporation into the NifDK scaffold via substitution of its terminal -SH ligand with a Cys residue, the Mo-cluster is expected to be relatively inert, as the Cp* ligand tightly binds to its Mo atom, and the core S atoms occupy the remaining coordination sites on its Mo and Fe atoms.

A plausible pathway for the incorporated Mo-cluster to prepare a substrate-binding site for the observed catalytic activities is to remove a core S atom of the cluster. In this context, a recent structural analysis of NifDK suggests binding of N_2 to the M-cluster via removal of a μ_2-bridging S atom in the belt region, which 'frees up' the binding sites on the Fe

atoms bridged by the belt-S atom.[17] Such a mechanism is also used for capturing CO- and Se-bound states of the M-cluster[18–20] and CO- and O/N-bound states of the cofactor of the vanadium nitrogenase.[21,22] Although the synthetic Mo-cluster lacks one of the Fe-(μ_2-S)-Fe bridges in the native M-cluster, the overall structural similarity between the two clusters implies that the Mo-cluster can use a similar mechanism to generate a substrate-binding site via removal of a μ_2-S atom following core reduction.

It is interesting to note that the catalytic behavior of NifDK^{Mo}, which harbors the Mo-containing mimic of the cofactor, is clearly distinct from NifDK^{Fe6}, which harbors an Fe-only synthetic analog of the Mo-cluster (Figure 5). NifDK^{Mo} is roughly twice as active as NifDK^{Fe6} in the ATP-dependent reduction of C_2H_2 to C_2H_4 (Figure 5A). This observation is consistent with the fact that the Mo-cluster is a more faithful synthetic mimic of the M-cluster than the Fe6-cluster in terms of its heterometallic nature and, consequently, the likelihood that insertion of the Mo-cluster—a structural mimic of the M-cluster with both the ‘Mo-end’ and the ‘Fe-end’ in place—induces a conformational change of NifDK that more closely resembles that induced upon insertion of the native M-cluster. A more ‘correct’ conformational change of NifDK^{Mo} is crucial for a proper docking of this protein with NifH during catalysis, which in turn facilitates the ATP-dependent electron transfer and substrate reduction at the cofactor site.

Strikingly, contrary to a higher activity of NifDK^{Mo} than NifDK^{Fe6} in the ATP-dependent substrate reduction, the relative activities of the two proteins are reversed in the ATP-independent reduction of C_2H_2 (Figure 5B) and CN- (Figure 5C), with NifDK^{Fe6} having a 1.7- and 1.4-fold higher product yield, respectively, than NifDK^{Mo} in these reactions. A difference in the apparent initial activities of NifDK^{Mo} (~320 nmol C_2H_4/mg protein/min) and NifDK^{Fe6} (~2300 nmol C_2H_4/mg protein/min) by one order of magnitude could very well reflect a significantly higher electron flux through NifDK^{Fe6} than that through NifDK^{Mo} when Eu^{II}-DTPA is used as a reducing agent. Taken together, the observation of disparate reactivities of NifDK^{Mo} and NifDK^{Fe6} is important, as it suggests that the incorporated clusters possess distinctive chemical properties that could be ‘tuned’ within the protein scaffold, a feature that could be explored in future protein engineering efforts.

CONCLUSION

In this study, we generated a novel semi-artificial enzyme, NifDK^{Mo}, by combining a synthetic, Mo-containing mimic of the M-cluster with the cofactor-free, NifDK protein scaffold. Excitingly, NifDK^{Mo} is capable of ATP-dependent and ATP-independent reduction of C_2H_2 to C_2H_4, and ATP-independent reduction of CN^- to short-chain hydrocarbons, under ambient conditions. Moreover, NifDK^{Mo} displays catalytic behaviors different than those of NifDK^{Fe6}, another semi-artificial enzyme that contains an all-Fe analog of the Mo-cluster within the NifDK protein scaffold. While the exact structures of these semi-artificial enzyme and their associated cofactors are yet to be elucidated, the apparent difference between the substrate-reducing activities of NifDK^{Mo} and NifDK^{Fe6} points to the possibility of using molecular design and cluster synthesis strategies to further develop semi-artificial or artificial systems[23–25] with desired catalytic activities, such as an activity of N_2 reduction at ambient conditions.[26] Our future studies will focus on the investigations

into the electronic and structural properties of these semi-artificial enzymes in hopes of informing future designs of nitrogenase-based catalysts for the production of useful chemical commodities.

EXPERIMENTAL SECTION

Unless otherwise specified, all chemicals were purchased from Sigma-Aldrich (St. Louis, MO) and Thermo Fisher Scientific (Waltham, MA).

General Procedures for Chemical Experiments.

All reactions were conducted under N_2 atmosphere using Schlenk techniques and a glove box (O_2 <1 ppm). Solvents were purified before use by passing them through columns of activated alumina and a supported copper catalyst.[13] The $[Cp^*MoFe_5S_9(SH)]^{3-}$ compound (designated Mo-cluster) was synthesized as described previously.[13]

General Procedures for Biochemical Experiments.

Unless otherwise noted, all procedures were carried out under Ar atmosphere using Schlenk techniques and a glove box (O_2 <1 ppm). The C_2H_2 gas was purchased from Praxair (Danbury, CT), and $Na^{13}CN$ was purchased from Cambridge Isotope Laboratories (Andover, MA). Eu^{II}-DTPA (Eu, europium; DTPA, diethylenetriamine pentaacetate) was prepared as discribed earlier.[15]

Cell Growth and Protein Purification.

Azotobacter vinelandii strains expressing His-tagged wild-type NifDK (DJ1141), non-tagged wild-type NifH (DJ1141), and His-tagged cofactor-deficient NifDK (DJ1143) were grown and harvested as previously discribed.[12,13] His-tagged NifDK, His-tagged cofactor-deficient NifDK (designated $NifDK^{apo}$) and non-tagged NifH were purified according to the procedures described earlier.[27,28]

Reconstitution of $NifDK^{apo}$ with Mo-cluster.

A DMF solution of Mo-cluster (2 mM, 319 μL; 638 nmol total) was added dropwise to a solution of $NifDK^{apo}$ (15 mg, 6.1 mL; 64 nmol total) containing 2 mM $Na_2S_2O_4$, 500 mM NaCl, 10% (v/v) glycerol, and 25 mM Tris-HCl (pH 8.0). The mixture was incubated at room temperature for 30 min before it was diluted with 3.0 mL EQ Buffer containing 25 mM Tris-HCl (pH 8.0), 500 mM NaCl, 10% (v/v) glycerol, and 2 mM $Na_2S_2O_4$. Subsequently, the diluted reaction mixture was loaded on a column packed with 1.5 mL EQ Buffer-equilibrated Ni Sepharose High Performance resin (GE Healthcare, Pittsburgh, PA), which allowed binding of the His-tagged, Mo-cluster-reconstituted $NifDK^{apo}$ (designated $NifDK^{Mo}$). The column was then washed with 3 mL EQ Buffer containing 20 mM β-mercaptoethanol, followed by elution of $NifDK^{Mo}$ from the column by 5 mL KO Buffer containing 25 mM Tris-HCl (pH 8.0), 500 mM NaCl, 10% (v/v) glycerol, 2 mM $Na_2S_2O_4$, and 250 mM Imidazole.

Inductively Coupled Plasma Optical Emission Spectroscopy (ICP-OES).

Fe and Mo contents were determined by inductively coupled plasma optical emission spectroscopy (ICP-OES) as described previously.[12]

Substrate Reduction Assays.

The ATP-dependent and ATP-independent C_2H_2 reduction assays were performed as described in detail earlier.[12] The CN^- reduction assays were carried out as previously outlined.[12] The ^{13}C-labeled and unlabeled products of the ATP-independent CN^- reduction assays, including CH_4, C_2H_4, C_2H_6, C_3H_6 and C_3H_8, were identified by gas chromatography-mass spectroscopy (GC-MS) analysis using Thermo Scientific TRACE 1300 gas chromatograph equipped with a Thermo Scientific ISQ QD single quadruple mass spectrometer (Thermo Electron North America LLC, Madison, WI). For each analysis, 250 μL of headspace was injected onto an Agilent PLOT/Q capillary column (0.32 mm diameter, 30 m length; Agilent Technologies, Santa Clara, CA), which was held at 40°C for 1 min, heated to 180°C at 10°C/min, and held at 180°C for 1 min.

X-ray Absorption Spectroscopy.

Fe and Mo K-edge X-ray absorption spectra were measured at SSRL beam line 7–3 using a 30-element solid-state Ge detector (Canberra) with a SPEAR3 storage ring current of ~500 mA at an energy of 3.0 GeV. The BL7–3 optics consists of a flat, bent, harmonic rejection vertically collimating Rh-coated Si M_0 mirror, and a liquid nitrogen cooled double crystal Si(220) monochromator. All Fe K-edge scans were taken between 6882 and 8000 eV, and all Mo K-edge scans were taken between 19760 and 20900 eV, with the samples maintained at ~10 K using an Oxford Instruments CF1208 continuous flow liquid helium cryostat cooled by an open-cycle He dewar. For Fe scans, fluorescence from an iron foil indirectly irradiated by scattered x-ray beam from a Kapton film placed prior to the ionization chamber I_0 and measured with a photodiode and scanned concomitantly for energy calibration, was used with the first inflection point of the edge assigned to 7112.0 eV. For Mo scans, a Mo standard was placed between the ionization chambers I_1 and I_2 and scanned concomitantly for energy calibration, with the first inflection point of the edge assigned to 20003.8 eV. Photoreduction was monitored by scanning the same spot on the sample twice and comparing the first derivative peaks associated with the edge energy during data collection. A Soller slit with 3 μm Mn and 6 μm Nb filters were used to improve the signal-to-noise ratio for the Fe and Mo K-edge data, respectively.

The detector channels from the scans were examined, calibrated, averaged, and processed for EXAFS analysis using EXAFSPAK[29] to extract $\chi(k)$. The Fe K-edge EXAFS data for the reconstituted *Av* NifDK samples were collected and processed without subtracting contributions of $NifDK^{apo}$. Theoretical phase and amplitude parameters for a given absorber-scatterer pair were calculated using FEFF 8.40[30] and subsequently applied to the nonlinear least squares ‘opt’ fitting program of the EXAFSPAK package during curve fitting. Parameters for each species were calculated using an appropriate model derived from the crystal structure of the synthetic Mo-cluster.[13] In all analyses, the coordination number of a given shell (N) was a fixed parameter and was varied iteratively in integer steps, whereas the bond length (R) and mean-square deviation (σ^2) were allowed to freely

float. The estimated uncertainties of R, σ^2, and N are 0.02 Å, 0.1×10^{-3} Å^2, and 20%, respectively. The amplitude reduction factor S_0 was fixed at 1.0 for all K-edge data, whereas the edge-shift parameter ΔE_0 was allowed to float as a single value for all shells. Thus, in any given fit, the number of floating parameters was typically equal to 2×number of shells+1. The goodness of fit (GOF) parameters were calculated as follows:

$$F = \sqrt{\sum k^6 \left(\chi_{\mathrm{exp}} - \chi_{calc}\right)^2}$$

$$F' = \sqrt{\sum k^6 \left(\chi_{\mathrm{exp}} - \chi_{calc}\right)^2 / \sum k^6 \chi_{\mathrm{exp}}{}^2}$$

Supplementary Material

Refer to Web version on PubMed Central for supplementary material.

Acknowledgements

This work was supported by NSF grant CHE-1904131 (M.W.R. and Y.H.) with regard to the GC-MS analyses and activity assays of hydrocarbon formation by NifDK^{Mo}, and NIH-NIGMS grant GM67626 (M.W.R. and Y.H.) with regard to the incorporation and spectroscopic characterization of the Mo-cluster in the NifDK scaffold. Y.O. and K.T. were supported by Grant-in-Aids for Scientific Research from the Ministry of Education, Culture, Sports, Science and Technology, Japan, No. 19H02733, 20K21207, and 21H00021 (Y.O.), and No. 23000007 and 21K20557 (K.T.), CREST grant from JST, Japan, No. JPMJCR21B1 (Y.O.), Kyoto University Research Fund for Young Scientist (Start-Up) (K.T.), and the International Collaborative Research Program of Institute for Chemical Re-search, Kyoto University. Y.O. was also supported by Takeda Science Foundation, the Yazaki Memorial Foundation, and Tatematsu Foundation. Stanford Synchrotron Radiation Lightsource, SLAC National Accelerator Laboratory, is supported by the U.S. Department of Energy, Office of Science, Office of Basic Energy Sciences under Contract No. DE-AC02-76SF00515. The SSRL Structural Molecular Biology Program is supported by the DOE Office of Biological and Environmental Research, and by the National Institutes of Health, National Institute of General Medical Sciences (P30GM133894) (K.H., B.H.).

This work is dedicated to Prof. Richard H. Holm.

References

[1]. Rees DC, Annu. Rev. Biochem 2002, 71, 221. [PubMed: 12045096]

[2]. Burgess BK, Lowe DJ, Chem. Rev 1996, 96, 2983. [PubMed: 11848849]

[3]. Buscagan TM, Rees DC, Joule 2019, 3, 2662. [PubMed: 32864580]

[4]. Rutledge HL, Tezcan FA, Chem. Rev 2020, 120, 5158. [PubMed: 31999100]

[5]. Jasniewski AJ, Lee CC, Ribbe MW, Hu Y, Chem. Rev 2020, 120, 5107. [PubMed: 32129988]

[6]. Lancaster KM, Roemelt M, Ettenhuber P, Hu Y, Ribbe MW, Neese F, Bergmann U, DeBeer S, Science 2011, 334, 974. [PubMed: 22096198]

[7]. Spatzal T, Aksoyoglu M, Zhang L, Andrade SLA, Schleicher E, Weber S, Rees DC, Einsle O, Science 2011, 334, 940. [PubMed: 22096190]

[8]. Christiansen J, Goodwin PJ, Lanzilotta WN, Seefeldt LC, Dean DR, Biochemistry 1998, 37, 12611. [PubMed: 9730834]

[9]. Schmid B, Ribbe MW, Einsle O, Yoshida M, Thomas LM, Dean DR, Rees DC, Burgess BK, Science 2002, 296, 352. [PubMed: 11951047]

[10]. Tanifuji K, Ohki Y, Chem. Rev 2020, 120, 5194. [PubMed: 32459087]

[11]. Hagen KS, Watson AD, Holm RH, J. Am. Chem. Soc 1983, 105, 3905.

[12]. Tanifuji K, Lee CC, Ohki Y, Tatsumi K, Hu Y, Ribbe MW, Angew. Chem. Int. Ed 2015, 54, 14022.

[13]. Tanifuji K, Sickerman NS, Lee CC, Nagasawa T, Miyazaki K, Ohki Y, Tatsumi K, Hu Y, Ribbe MW, Angew. Chem. Int. Ed 2016, 55, 15633.

[14]. Ljones T, Burris RH, Biochemistry 1978, 17, 1866. [PubMed: 656366]

[15]. Vincent KA, Tilley GJ, Quammie NC, Streeter I, Burgess BK, Cheesman MR, Armstrong FA, Chem. Commun 2003, 20, 2590.

[16]. Van Der Laan GP, Beenackers AACM, Catal. Rev 1999, 41, 255.

[17]. Kang W, Lee CC, Jasniewski AJ, Ribbe MW, Hu Y, Science 2020, 368, 1381. [PubMed: 32554596]

[18]. Spatzal T, Perez KA, Einsle O, Howard JB, Rees DC, Science 2014, 345, 1620. [PubMed: 25258081]

[19]. Buscagan TM, Perez KA, Maggiolo AO, Rees DC, Spatzal T, Angew. Chem. Int. Ed 2021, 60, 5704.

[20]. Spatzal T, Perez KA, Howard JB, Rees DC, Elife 2015, 4, e11620. [PubMed: 26673079]

[21]. Sippel D, Rohde M, Netzer J, Trncik C, Gies J, Grunau K, Djurdjevic I, Decamps L, Andrade SLA, Einsle O, Science 2018, 359, 1484. [PubMed: 29599235]

[22]. Rohde M, Grunau K, Einsle O, Angew. Chem. Int. Ed 2020, 59, 23626.

[23]. Hemschemeier A, Happe T, Nat. Rev. Chem 2018, 2, 231.

[24]. Schwizer F, Okamoto Y, Heinisch T,Gu Y, Pellizzoni MM, Lebrun V, Reuter R, Köhler V, Lewis JC, Ward TR, Chem. Rev 2018, 118, 142. [PubMed: 28714313]

[25]. Mirts EN, Bhagi-Damodaran A, Lu Y, Acc. Chem. Res 2019, 52, 935. [PubMed: 30912643]

[26]. Ohki Y, Uchida K, Tada M, Cramer RE, Ogura T, Ohta T, Nat. Commun 2018, 9, 3200. [PubMed: 30097563]

[27]. Ribbe MW, Hu Y, Guo M, Schmid B, Burgess BK, J. Biol. Chem 2002, 277, 23469. [PubMed: 11978793]

[28]. Bursey EH, Burgess BK, J. Biol. Chem 1998, 273, 16927. [PubMed: 9642255]

[29]. George GN, In EXAFSPAK: A suite of computer programs for analysis of X-ray absorption spectra, 1990.

[30]. Ankudinov AL, Ravel B, Rehr JJ, Conradson SD, Phys. Rev. B 1998, 58, 7565.

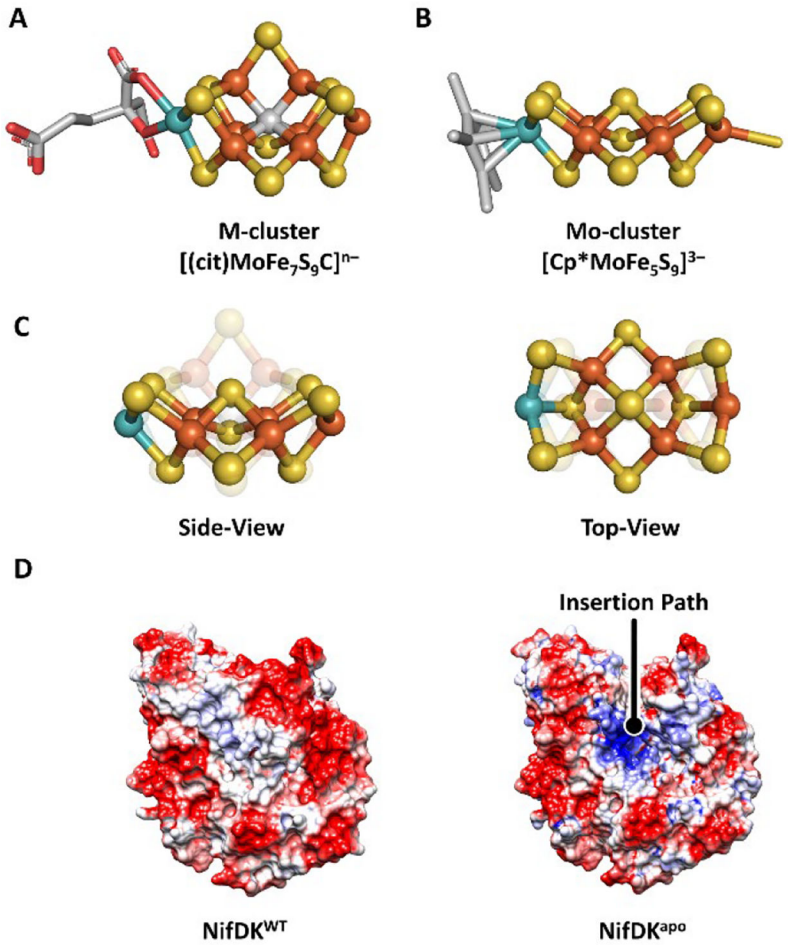

Figure 1.

Crystal structures of (**A**) M-cluster (PDB ID: 3U7Q) and (**B**) Mo-cluster ($[Cp^*MoFe_5S_9(SH)]^{3-}$; Cp*, C5Me5, where Me refers to methyl),[13] (**C**) side- and top-views of overlaid structures of M- and Mo-clusters, and (**D**) electrostatic surface representations of the wild-type NifDK ($NifDK^{WT}$) and the cofactor-deficient NifDK ($NifDK^{apo}$). Color codes in A-C: C, light gray; Fe, orange; Mo, teal; O, red; S, yellow. Negative and positive potentials in D are shown in red and blue, respectively.

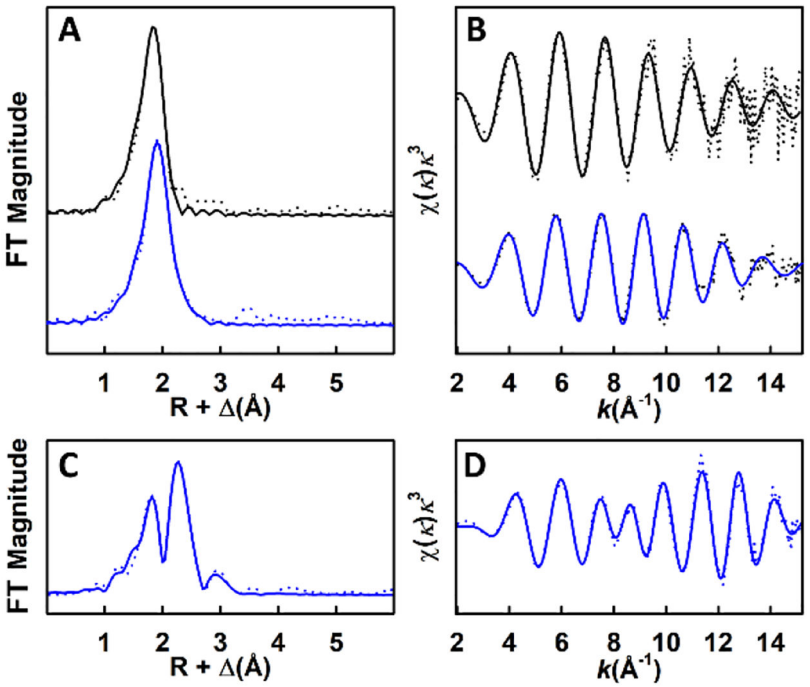

Figure 2.

Fe (**A**, **B**) and Mo (**C**, **D**) K-edge EXAFS data (dotted) and best fits (solid) of $NifDK^{apo}$ (black) and $NifDK^{Mo}$ (blue). Shown are the k^3-weighted EXAFS data (A, C) and the Fourier transformed EXAFS data (B, D). See Supporting Information (Tables S1–S3) for details of fits.

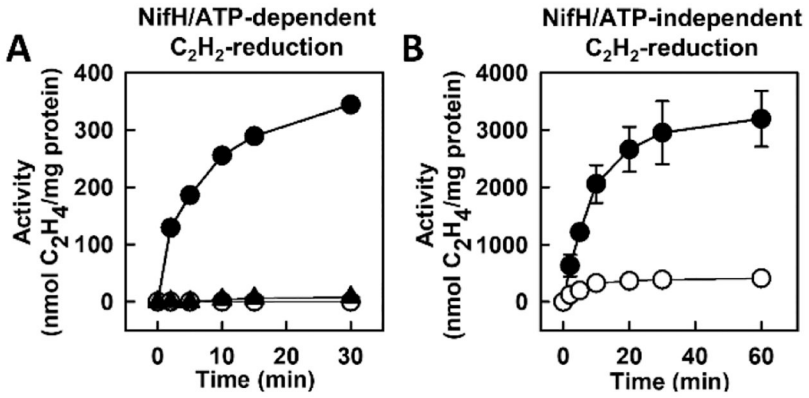

Figure 3.

Reduction of C2H2 to C2H4 by NifKMo (-●-) in the presence (**A**) or absence (**B**) of ATP and NifH, and controls with $NifDK^{Mo}$ but no ATP (-○-) (A) or no NifH (-▲-) (A), and with $NifDK^{apo}$ (-○-) but no ATP and NifH (B). The NifH/ATP-dependent assays (A) contained dithionite as a reductant, and the NifH/ATP-independent assays (B) contained Eu(II)-DTPA as reductant.

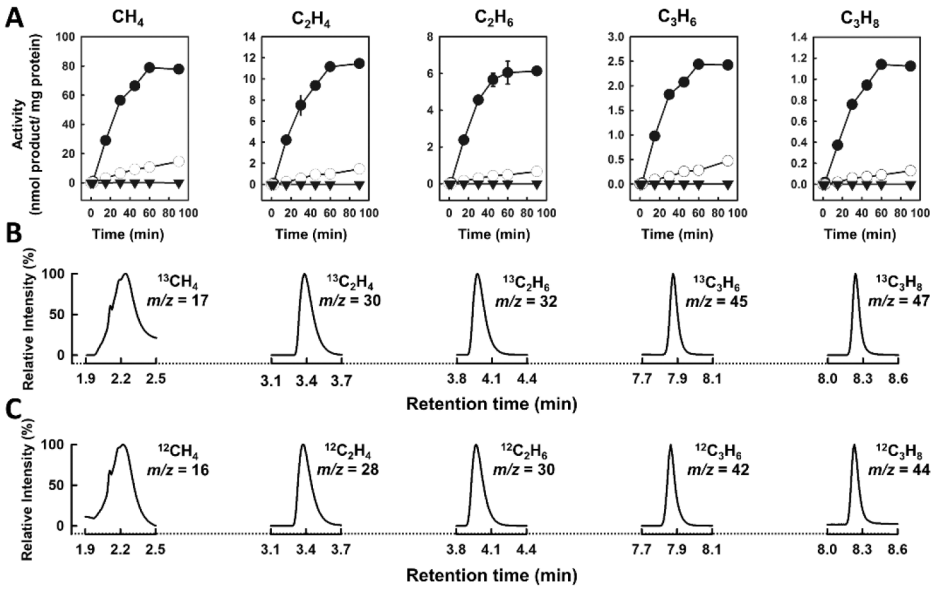

Figure 4.

(**A**) ATP-independent reduction of CN^- to C_1-C_3 hydrocarbons in reactions containing $NifDK^{Mo}$ (-●-), $NifDK^{apo}$ (-○-), or no protein (-▼-). GC-MS analysis of hydrocarbon products generated from $^{13}CN^-$ (**B**) and unlabeled CN^- (**C**) in reactions containing $NifDK^{Mo}$. All reactions contained EuII-DTPA as a reductant. The small amount of hydrocarbon formation by the cofactor-deficient $NifDK^{apo}$ (-○-) likely originated from the P-cluster species in this protein.

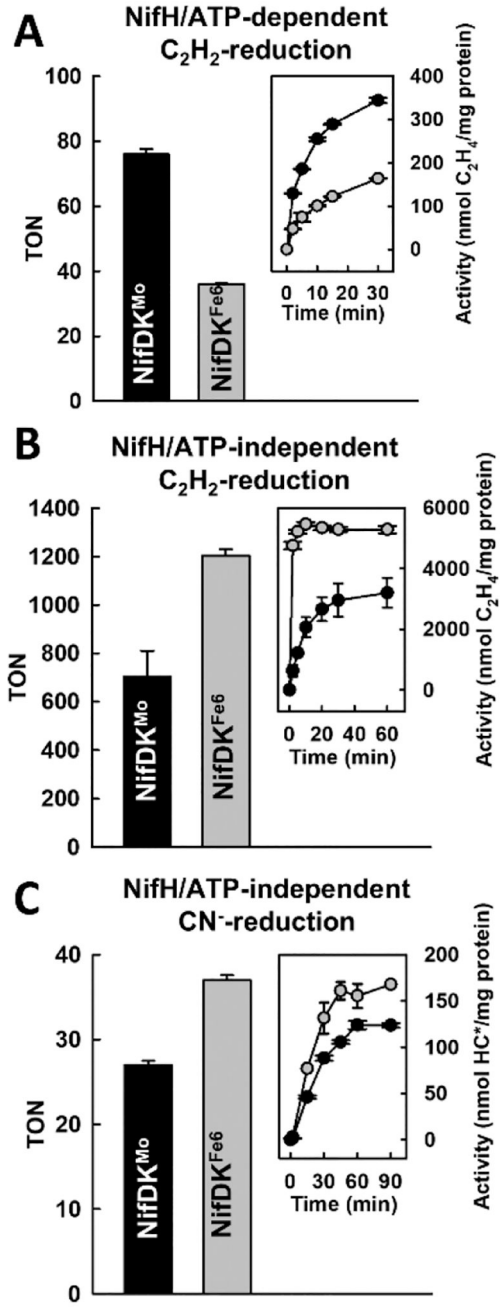

Figure 5.

ATP-dependent reduction of C_2H_2 (**A**) and ATP-independent reduction of C_2H_2 (**B**) and CN^- (**C**) by $NifDK^{Fe6}$ (gray bars and spheres) and $NifDK^{Mo}$ (black bars and spheres). Shown are TONs (bars) and time courses (insets) of the reactions. The TONs and activities of $NifDK^{Fe6}$ are taken from Ref. 12. The TON and activity of hydrocarbon (HC) formation by $NifDK^{Mo}$ in the ATP-dependent reaction of CN^- reduction (C) were calculated from data presented in Figure 4A and represent the total amount of reduced C atoms in all hydrocarbon products.